Acoustics Australia
https://doi.org/10.1007/s40857-021-00218-5

ORIGINAL PAPER

Application of a Chebyshev Collocation Method to Solve a Parabolic Equation Model of Underwater Acoustic Propagation

Yongxian Wang[1] · Houwang Tu[1] · Wei Liu[1] · Wenbin Xiao[1] · Qiang Lan[1]

Received: 5 December 2020 / Accepted: 4 February 2021

Abstract
The parabolic approximation has been used extensively for underwater acoustic propagation and is attractive because it is computationally efficient. Widely used parabolic equation (PE) model programs such as the range-dependent acoustic model (RAM) are discretized by the finite difference method. Based on the idea of the Padé series expansion of the depth operator, a new discrete PE model using the Chebyshev collocation method (CCM) is derived, and the code (CCMPE) is developed. Taking the problems of four ideal fluid waveguides as experiments, the correctness of the discrete PE model using the CCM to solve a simple underwater acoustic propagation problem is verified. The test results show that the CCMPE developed in this article achieves higher accuracy in the calculation of underwater acoustic propagation in a simple marine environment and requires fewer discrete grid points than the finite difference discrete PE model. Furthermore, although the running time of the proposed method is longer than that of the finite difference discrete PE program (RAM), it is shorter than that of the Chebyshev–Tau spectral method.

Keywords Chebyshev collocation method · Spectral method · Parabolic equation model · Underwater acoustics

1 Introduction

Research on underwater acoustic propagation modeling theory began in the 1960s. Initially, only ray theory and the horizontally layered normal mode theory existed. Their ability to deal with problems was limited, and they could only calculate range-independent problems. Since the 1970s, parabolic equation (PE) models have emerged that can address range-dependent two-dimensional sound propagation problems [1]. The PE model is a parabolic approximation of the wave equation. It was first used to solve the problem of radio wave propagation in the atmosphere and was then gradually applied to branch disciplines in physics, including optics, plasma physics, seismology and underwater acoustics.

In 1977, Tappert [2] introduced the PE model to underwater acoustics for the first time, and he approximated the Helmholtz equation as a two-dimensional equation that was related only to the range and depth and not the azimuth. Since then, research on PE models in underwater acoustics has gradually increased. From the introduction of PEs in underwater acoustics to the 1980s, the related research on PEs focused mainly on theoretical models [3] and numerical solutions [4,5]. From the 1980s to the 1990s, PEs entered a period of rapid development, and a large number of research results appeared, including the development of various PE models (three-dimensional PEs [6], elastic PEs [7], high-order PEs [8], wide-angle PEs [9], etc.) as well as the processing of boundary conditions [7], the initial conditions of PEs [10] and the study of phase error and PE computational methods [11]. Since then, the research related to PEs has focused mainly on theories [12] and PE programs [13–15]. A more detailed development history can be found in [16].

The widely used numerical calculation PE-based programs have primarily been developed using the finite difference method (FDM). In obtaining the numerical solutions of partial differential equations in engineering, the spectral method is a reliable option and has been widely used in various engineering technology fields [17,18]. The collocation method is a special spectral method; when forming algebraic equations, it does not use a weak form of differential equa-

✉ Yongxian Wang
yxwang@nudt.edu.cn

Houwang Tu
tuhouwang96@163.com

[1] College of Meteorology and Oceanography, National University of Defense Technology, Changsha, China

Published online: 22 February 2021

tions as in other spectral methods but directly adopts a strong form, so the original differential equation is strictly established at the collocation points [19]. The collocation method has the advantages of high precision and high speed and is widely used in the field of engineering technology [20–23]. In recent years, some scholars have attempted to introduce spectral methods, including the collocation method, to the problem of underwater sound propagation. Evans proposed a Legendre–Galerkin technique for differential eigenvalue problems with complex and discontinuous coefficients based on normal modes [24]. Tu et al. presented normal mode and standard PE models using the Chebyshev–Tau spectral method to process a single layer of a body of water with constant density and no attenuation [25]. They then extended this method to solve the problem of a layered marine environment [26,27] and subsequently presented a Chebyshev-Tau spectral method for a PE model with wide-angle rational approximation [28]. Colbrook et al. analyzed a spectral collocation method for acoustic scattering by multiple elastic plates [29]. These studies have shown that the collocation method has high accuracy in the calculation of underwater acoustic propagation, and the high-precision underwater acoustic field is the basis of the underwater matching field positioning and the inversion of geoacoustic parameters. Therefore, the collocation method has great potential value in computational underwater acoustics. In this article, we introduce a Chebyshev collocation method (CCM) for the solution of a PE model in underwater acoustics, design several experiments and analyze and compare the advantages and shortcomings of the CCM-based PE model proposed in this paper in terms of its computational accuracy and speed.

2 Parabolic Equation Model for An Underwater Acoustic Propagation Problem

Considering a range-independent marine environment, the governing wave equation of underwater acoustic propagation in the frequency domain can be written as the following Helmholtz equation [1]:

$$(\nabla^2 + k^2)\tilde{P} = 0, \tag{1}$$

where $k = \omega/c$ is the wavenumber, $\omega = 2\pi f$ is the angular frequency, f is the frequency of the sound source, c is the sound speed and $\tilde{P}$ is the sound pressure in the frequency domain. Considering a cylindrical coordinate system where the sound source is a simple harmonic point source and the marine environment is a cylindrically symmetric two-dimensional sound propagation case, the Helmholtz equation (1) can be expressed as [1,14] :

$$\left[\frac{\partial^2}{\partial r^2} + \frac{1}{r}\frac{\partial}{\partial r} + \rho\frac{\partial}{\partial z}\left(\frac{1}{\rho}\frac{\partial}{\partial z}\right) + k_0^2 n^2\right]\tilde{P} = 0, \tag{2}$$

where c_0 is the reference sound speed, $k_0 = \omega/c_0$ represents the reference wavenumber and $n = c_0/c$ represents the refractive index. Note that the sound pressure $\tilde{P} \equiv \tilde{P}(\omega; r, z)$ depends on the spatial position (r, z) (and the angular frequency ω). For long-distance sound propagation, sound waves are generally approximated as cylindrical waves. According to the attenuation law of cylindrical waves, the energy amplitude of the sound wave is proportional to $\sqrt{r}$. To eliminate the extension term, the following variable transformation is introduced:

$$p = \sqrt{r}\tilde{P} \tag{3}$$

By substituting Eq. (3) into Eq. (2), we obtain:

$$\frac{\partial^2 p}{\partial r^2} + \rho\frac{\partial}{\partial z}\left(\frac{1}{\rho}\frac{\partial p}{\partial z}\right) + k_0^2 n^2 p + \frac{p}{4r^2} = 0. \tag{4}$$

Applying the so-called "far-field approximation" yields $k_0^2 n^2 p \gg \frac{p}{4r^2}$. When $k_0 r \gg 1$ is applied to Eq. (4), we have:

$$\frac{\partial^2 p}{\partial r^2} + \rho\frac{\partial}{\partial z}\left(\frac{1}{\rho}\frac{\partial p}{\partial z}\right) + k_0^2 n^2 p = 0. \tag{5}$$

When ignoring the horizontal change in the medium parameter, Eq. (5) can be factorized as the product of two operators representing the outwardly propagating waves and inwardly propagating waves:

$$\left(\frac{\partial}{\partial r} - ik_0\sqrt{1+\mathcal{X}}\right)\left(\frac{\partial}{\partial r} + ik_0\sqrt{1+\mathcal{X}}\right)p = 0, \tag{6}$$

where the depth operator $\mathcal{X}$ is:

$$\mathcal{X} = k_0^{-2}\left[\rho\frac{\partial}{\partial z}\left(\frac{1}{\rho}\frac{\partial}{\partial z}\right) + k^2 - k_0^2\right]. \tag{7}$$

The operator appearing in the first pair of parentheses of Eq. (6) represents the waves propagating outwards, and the operator appearing in the second pair of parentheses represents the waves propagating inwards. When the inward propagation can be considered negligible, we can obtain a parabolic equation of the following form:

$$\frac{\partial p}{\partial r} = ik_0\sqrt{1+\mathcal{X}}p. \tag{8}$$

According to the method of solving ordinary differential equations, the step solution of Eq. (8) can be obtained as:

$$p(r+\Delta r,z)=\exp\left(ik_0\Delta r\sqrt{1+\mathcal{X}}\right)p(r,z), \tag{9}$$

where Δr is the step size in the distance direction. To address the exponential and/or square-root expression of the linear operator $\mathcal{X}$ appearing in Eq. (9), a Padé series expansion method was introduced by Collins [8], which uses an n-term rational function to approximate the exponential function in Eq. (9):

$$p(r+\Delta r,z)\approx\exp\left(ik_0\Delta r\right)\prod_{j=1}^{n}\frac{1+\alpha_{j,n}\mathcal{X}}{1+\beta_{j,n}\mathcal{X}}p(r,z). \tag{10}$$

The calculation of the complex coefficients $\alpha_{j,n}$ and $\beta_{j,n}$ needs to meet the requirements of stability, convergence and accuracy.

To solve Eq. (10) numerically, the depth operator $\mathcal{X}$ needs to be discretized. Traditionally, the FDM is usually used to discretize the depth operator and ultimately form a set of tridiagonal-matrix algebraic equations. This article uses the CCM to solve PE problems.

3 Chebyshev Collocation Method for the PE Model

3.1 Chebyshev Collocation Method

Eq. (10) can be discretized by the CCM. The collocation method is a kind of spectral method that is based on the principle of weighted residual minimization. In the next section, a brief description of the fundamentals of the method of weighted residuals and the CCM is presented, and a more detailed and rigorous derivation can be found elsewhere; see [30].

We show the process of solving equations using the spectral method by using a one-dimensional differential equation boundary value problem:

$$\begin{aligned}&\mathcal{L}u(x)-f(x)=0,\quad x\in D\backslash\partial D\\&\mathcal{B}u(x)-g(x)=0,\quad x\in\partial D\end{aligned} \tag{11}$$

where $\mathcal{L}$ is a differential operator, $u(x)$ is an unknown function, D is the definite domain, $\mathcal{B}$ is a linear boundary operator and ∂D is the boundary of D. In the method of weighted residuals, a set of linearly independent basis functions are selected to expand the unknown function, as follows:

$$u(x)=\sum_{k=0}^{\infty}a_k\phi_k(x), \tag{12}$$

where a_k is the expansion coefficient and $\phi_k(x)$ is the basis function. In actual numerical calculations, the basis function cannot be infinite, so it must be truncated to $(N+1)$ basis functions, as shown in the following formula:

$$u(x)\approx\hat{u}(x)=\sum_{k=0}^{N}a_k\phi_k(x). \tag{13}$$

When the expanded $u(x)$ is brought into Eq. (11), (11) no longer strictly holds, and the following residuals $R(x)$ arise:

$$R(x)=\mathcal{L}\hat{u}(x)-f(x). \tag{14}$$

The constraint on the expansion coefficients is satisfied by letting the weighted residuals be 0:

$$\int_D R(x)w_j(x)\mathrm{d}x=0,\quad j=0,1,2,\ldots N, \tag{15}$$

where $w_j(x)$ is the weight function and the expansion coefficients can be obtained with Eq. (15). Thus, the choice of the basis function set $\{\phi_k(x)\}$ and weight function set $\{w_j(x)\}$ are very important. The collocation method is a spectral method that uses the δ functions as the weight function:

$$\begin{aligned}&\int_D R(x)\delta(x-x_j)\mathrm{d}x=R(x_j)=\mathcal{L}\hat{u}(x_j)-f(x_j)=0,\\&j=0,1,2,\ldots N,\end{aligned} \tag{16}$$

where x_j is the j-th point of the $(N+1)$ discrete grid points in D. Based on the above formula, the collocation method essentially only requires the weighted residuals to be 0 at discrete points, and the equations formed for solving the unknown functions are in a physical space instead of a spectral space (as in the case of other spectral methods such as those of Tau and Galerkin). In other words, the collocation method requires that the original equation is strictly established only on discrete grid points x_j and not on other points in D. The basis function of the CCM is the Chebyshev orthogonal polynomial [19], which can be defined on the interval $x\in[-1,1]$ as follows:

$$T_k(x)=\cos(k\theta),\quad \theta=\arccos x,\quad x\in[-1,1]. \tag{17}$$

In the CCM, the $(N+1)$ discrete grid points x_j on the interval $[-1,1]$ can be taken as nonequidistant Chebyshev–Gauss–Lobatto (CGL) collocation grid points:

$$x_j=\cos\left(\frac{j\pi}{N}\right),\quad j=0,1,2\ldots,N. \tag{18}$$

The CGL points correspond to the extreme points of the Chebyshev polynomials [31]. If $x \in [a, b]$, we give the following more general form of Eqs. (17) and (18):

$$\begin{aligned} T_k(x) &= \cos(k\theta), \quad \theta = \arccos\left(\frac{2}{b-a}x - \frac{b+a}{b-a}\right), \quad x \in [a, b] \\ x_j &= \frac{a-b}{2}\cos\left(\frac{j\pi}{N}\right) + \frac{b+a}{2}, \quad j = 0, 1, 2 \ldots, N \end{aligned} \tag{19}$$

During the solution process of the CCM, any function defined on the domain $[a, b]$ can be discretized as its values at the $(N+1)$ CGL points and thus can be expressed as an $(N+1)$-dimensional column vector, such as:

$$\begin{aligned} \mathbf{u} &= \left[u_0, u_1, u_2, \cdots, u_N\right]^T, \quad u_j = u(x_j), \\ \mathbf{f} &= \left[f_0, f_1, f_2, \cdots, f_N\right]^T, \quad f_j = f(x_j), \quad j = 0, 1, \ldots, N. \end{aligned} \tag{20}$$

To apply the CCM to the differential equation Eq. (11), the discretization of the operator $\mathcal{L}$ is necessary. This operator may contain derivatives and multiplications.

The derivative operator is usually included in the $\mathcal{L}$ operator. We give the relationship between the functions $u'(x)$ and $u(x)$ as follows:

$$\mathbf{u}' = \mathbf{D}\mathbf{u}. \tag{21}$$

Here, $\mathbf{u}' = [u'_0, u'_1, u'_2, \ldots, u'_N]^T$ represents the (discretized) function value of the derivative term $u'(x)$. Matrix $\mathbf{D}$, called the Chebyshev collocation differential matrix of $x \in [a, b]$, describes the relationship between the first derivative of the function and the original function in the CCM. The elements of matrix $\mathbf{D}$ can be expressed as:

$$\begin{aligned} D_{00} &= \frac{2N^2+1}{3(b-a)}, \quad D_{NN} = -\frac{2N^2+1}{3(b-a)}, \\ D_{jj} &= \frac{-x_j}{(b-a)(1-x_j^2)}, \quad j = 1, 2, 3, \cdots, N-1 \\ D_{ij} &= \frac{2c_i(-1)^{i+j}}{(b-a)(x_i - x_j)}, \quad i \neq j; \quad i, j = 0, 1, 2, \cdots, N; \\ c_i &= \begin{cases} 2, & i = 0, N \\ 1, & \text{otherwise} \end{cases} \end{aligned} \tag{22}$$

The reader is referred to Shen-Jie [30]; please note that there is a minor difference in the form of matrix $\mathbf{D}$ because of the different domains of the function u (either $[-1, 1]$ or $[a, b]$). The relationship between the second derivatives $u''(x)$ and $u(x)$ can be evaluated easily as $\mathbf{u}'' = \mathbf{D}^2\mathbf{u}$.

The discretization vector of the product function $y(x) = v(x)u(x)$ on $x \in [a, b]$ can be processed as follows in the CCM:

$$\mathbf{y} = \mathbf{C}_v\mathbf{u}, \tag{23}$$

where $\mathbf{C}_v$ is an $(N+1) \times (N+1)$ diagonal matrix and $(C_v)_{ii} = v_i = v(x_i), i = 0, 1, \ldots, N$.

In this way, the differential equation can be discretized into a system of algebraic equations, and the problem can be solved. In the process of carrying out the programming implementation, the unknown function $u(x)$ is not necessarily expanded with Chebyshev polynomials but makes the original equation strictly true at the CGL points. Thus, a system of algebraic equations is formed, and the function value $u(x_j)$ at the CGL points x_j is ultimately obtained by solving the above equations. The function values of the remaining points on the interval $[a, b]$ can be obtained by interpolation after $u(x_j)$ is obtained.

A systematic theoretical study of the convergence of the Chebyshev polynomials and the collocation method is found in [19,32], and the asymptotic rate of convergence in the CCM has been reported previously; more details are provided in [33].

3.2 Discrete PE Model Using the CCM

In what follows, we use the CCM to numerically discretize the operator $\mathcal{X}$ in Eq. (7) and p in Eq. (10). We use $(N+1)$ CGL points and note that $z \in [0, H]$, so the matrix form of the depth operator $\mathcal{X}$ is:

$$\mathbf{X} = k_0^{-2}\left(\mathbf{C}_\rho\mathbf{D}\mathbf{C}_{1/\rho}\mathbf{D} + \mathbf{C}_{k^2} - k_0^2\mathbf{I}\right). \tag{24}$$

Here, $\mathbf{C}_\rho$, $\mathbf{C}_{1/\rho}$ and $\mathbf{C}_{k^2}$ are defined by Eq. (23) with $v = \rho$, $v = 1/\rho$ and $v = k^2$, respectively. $\mathbf{D}$ is defined in Eq. (21) (here $a = 0$, $b = H$), and $\mathbf{I}$ represents the identity matrix. As a result, the matrix form of Eq. (10) can be written as:

$$\mathbf{p}(r + \Delta r) = \exp(ik_0\Delta r)\prod_{j=1}^{n}\frac{\mathbf{I} + \alpha_{j,n}\mathbf{X}}{\mathbf{I} + \beta_{j,n}\mathbf{X}}\mathbf{p}(r). \tag{25}$$

In Eq. (25), $\mathbf{p}(r)$ is the column vector containing the $(N+1)$ function values of $\{p_{r,z_j}\}$ at the CGL points. In the CCM, the boundary conditions are processed by modifying the algebraic equations. When the sediment is not considered, the upper and lower boundaries of the PE model are actually pressure release boundaries; that is:

$$\tilde{P}(z = 0) = \tilde{P}(z = H) = 0. \tag{26}$$

It can be obtained from Eq. (3) that $p(z=0)=p(z=H)=0$, and the boundary conditions can be expressed as:

$$p_{r,z_0}=p_{r,z_N}=0. \tag{27}$$

The initial field $p(\cdot)$ near $r=0$ is obtained from the self-starter [10,14], and the full-field sound pressure $p(r,z)$ is obtained by step iteration. The distance r is increased by Δr at every forwarding step in the range direction, and it requires solving n linear systems, where each includes $(N+1)$ equations. Here, n is the order of the Padé series taken. The full-field sound pressure $p(r,z)$ at this time is at nonequidistant CGL points, and approximations of the solution at any other points can be easily interpolated from the CGL points.

To demonstrate the sound field results, the transmission loss (TL) of the sound pressure is defined as follows:

$$\mathrm{TL}=-20\log_{10}\left(\frac{|\tilde{P}|}{|\bar{P}|}\right). \tag{28}$$

Its unit is decibels (dB), where $\bar{P}$ is the sound pressure at a distance of 1 m from the sound source.

4 Numerical Experiments and Analysis

To verify the validity of the CCM in solving the PE model, the following analysis is performed through 4 experiments in Table 1. Figure 1 shows the sound speed profiles used in the numerical experiments. In the four ocean waveguides, the density of the seawater is uniform ($\rho(z)$=1 g/cm^3), and the speed of sound underwater is constant (c_0=1500 m/s).

To facilitate the description, the PE model program based on the CCM that we developed is abbreviated as CCMPE. The comparison programs in the experiments are the classic PE model program RAM and CSMPE (based on the Chebyshev–Tau spectral method [28]); in addition, the classic normal mode program KRAKEN [34] and fast field program (FFP) are included. The initial fields of the three PE-based programs in the article are obtained from the self-starter [10]. In CCMPE and CSMPE, the setting principles of both n (the number of terms of Padé approximation) and Δr (the step length in range direction) are consistent with the RAM [14].

4.1 Experiment 1: An Ideal Fluid Waveguide with a Constant Sound Speed Profile

The depth of the sea is H=100 m, the sound source is located at a depth of z_s=36 m, and the sound source frequency is 20 Hz. According to the wavenumber integration method, the exact analytical solution of the above ideal fluid waveguide is:

$$p(r,z)=\frac{2\pi i}{H}\sum_{m=1}^{\infty}\sin(k_{z_m}z_s)\sin(k_{z_m}z)H_0^{(1)}(k_{r_m}r)$$
$$k_{z_m}=m\pi/H,\quad k_{r_m}=\sqrt{k^2-k_{z_m}^2},\quad m=1,2,\ldots \tag{29}$$

where $H_0^{(1)}(\cdot)$ is a Hankel function of the first kind. Figure 2 shows the TL calculated using the analytical solution, RAM, CSMPE and CCMPE programs developed in this article. In the horizontal direction, Δr is 1 m. In the vertical direction, the distance between the discrete grid points of the RAM is 0.5 m—i.e., there are a total of 200 discrete points—while the CSMPE and CCMPE use 50 discrete points in the vertical direction, and the number of terms of the rational approximation coefficients is $n=8$. It can be seen from Fig. 2 that the TL fields calculated by the four schemes are very similar, with the exception of obvious differences within a horizontal distance of approximately 300 m. Compared with the analytical solution of Fig. 2a, it can be seen that under the near field, the results calculated by the RAM, CSMPE and CCMPE have some distortions, but the numbers of sound shadow areas are equal. This result may be due to the introduction of the so-called far-field approximation in the PE model. However, regarding the calculation results of the RAM and CSMPE, the overall fields are very similar, so the accuracy of the three programs needs to be compared further.

Figure 3a shows the TL curves calculated by all three methods together with the analytic result at a depth of 36 m. It can be seen from the figure that in the near field within 300 m from the source, the results of the RAM, CSMPE and CCMPE are significantly different from the analytical solution, but the differences among the RAM, CSMPE and CCMPE are small. In the far field, all four calculation results of the TL are very consistent, with the only exception being that there are inconspicuous differences in the sound shadow area, as shown in Fig. 3b. Figure 3c shows the errors between the RAM, CSMPE and CCMPE programs and the analytical solution. The calculation results of the three PE-based programs and the analytical solution differ greatly in the near field, but the error among the three is small, which illustrates that the near-field error is generated by the PE model itself and is unrelated to the discrete method during the calculation process. In the far field, as shown in Fig. 3d, the error of the CCMPE is smaller than that of the RAM and CSMPE, especially in the sound shadow areas.

Table 1 List of experiments

Experiment No.	Frequency (Hz)	Depth (m)	Source depth (m)	Sound speed profile
1	20	100	36	Figure 1a
2	20	150	40	Figure 1b
3	30	100	60	Figure 1c
4	50	5000	1000	Figure 1d

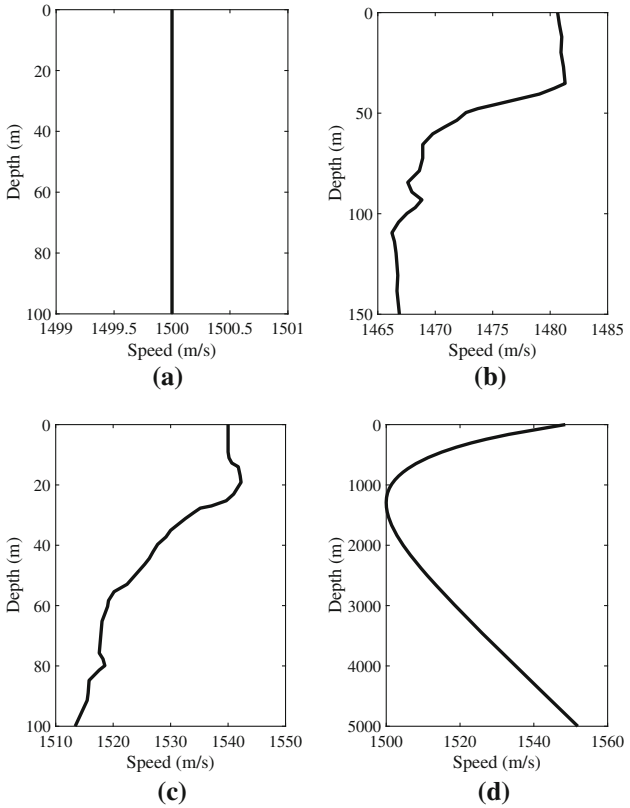

Fig. 1 Sound speed profiles in the experiments

4.2 Experiment 2: An Ideal Fluid Waveguide with a Barents Sea Sound Speed Profile

The sound speed profile in this experiment is the measured data from the Barents Sea provided by [35]. In this case, the depth of the sea is H=150 m, the sound source is located at a depth of z_s=40 m, and the sound source frequency is 20 Hz.

Figure 4 shows the TL calculated using the KRAKEN, RAM, CSMPE and CCMPE programs. Since there is no analytical solution for this experiment, we use KRAKEN's result as a reference. In the horizontal direction, Δr is 5 m. In the vertical direction, the distance of the discrete grid points of the RAM is 0.5 m, for a total of 300 discrete points, while CSMPE and CCMPE use 50 discrete points in the vertical direction, and the number of terms of the rational approximation coefficients is 8. It can be seen from Fig. 4 that the TL fields calculated by the four schemes are very similar, but there are slight differences within a horizontal distance of approximately 100 m. Figure 5 shows the TL calculated by the four schemes at a depth of 40 m. The results of the RAM, CSMPE and CCMPE are obviously different from those of the KRAKEN in the near field, but the differences among the RAM, CSMPE and CCMPE are indistinguishable. In the far field, the calculation results of the TL of the four schemes are completely consistent.

4.3 Experiment 3: An Ideal Fluid Waveguide with a Surface Duct Sound Speed Profile

The sound speed profile in this experiment is the set of measured data of a surface duct provided by [35]. In this case, the depth of the sea is H=100 m, the sound source is located at a depth of z_s=36 m, and the sound source frequency is 30 Hz.

Figure 6 shows the TL calculated using the KRAKEN, RAM, CSMPE and CCMPE programs in this experiment. There is no analytical solution for this experiment; we use KRAKEN's result as a reference. In the horizontal direction, Δr is 5 m. In the vertical direction, the distance of the discrete grid points of the RAM is 0.5 m, for a total of 200 discrete points, while CSMPE and CCMPE use 100 discrete points in the vertical direction, and the number of terms of the rational approximation coefficients is 8. It can be seen from Fig. 6 that the TL fields calculated by the four schemes are very similar, but there are differences within a horizontal distance of approximately 100 m. Figure 7 shows the TL calculated by the four schemes at a depth of 60 m. The results of the RAM, CSMPE and CCMPE are slightly different from those of the KRAKEN in the near field, but the differences among the RAM, CSMPE and CCMPE are almost completely indistinguishable in the far field, and the calculation results of the TL of the four schemes are extremely consistent.

4.4 Experiment 4: An Ideal Fluid Waveguide with a Munk Sound Speed Profile

The Munk profile is an idealized ocean sound speed profile that illustrates many features that are typical of deep water propagation [1]. In the last experiment, $n = 8$ and $f = 50$

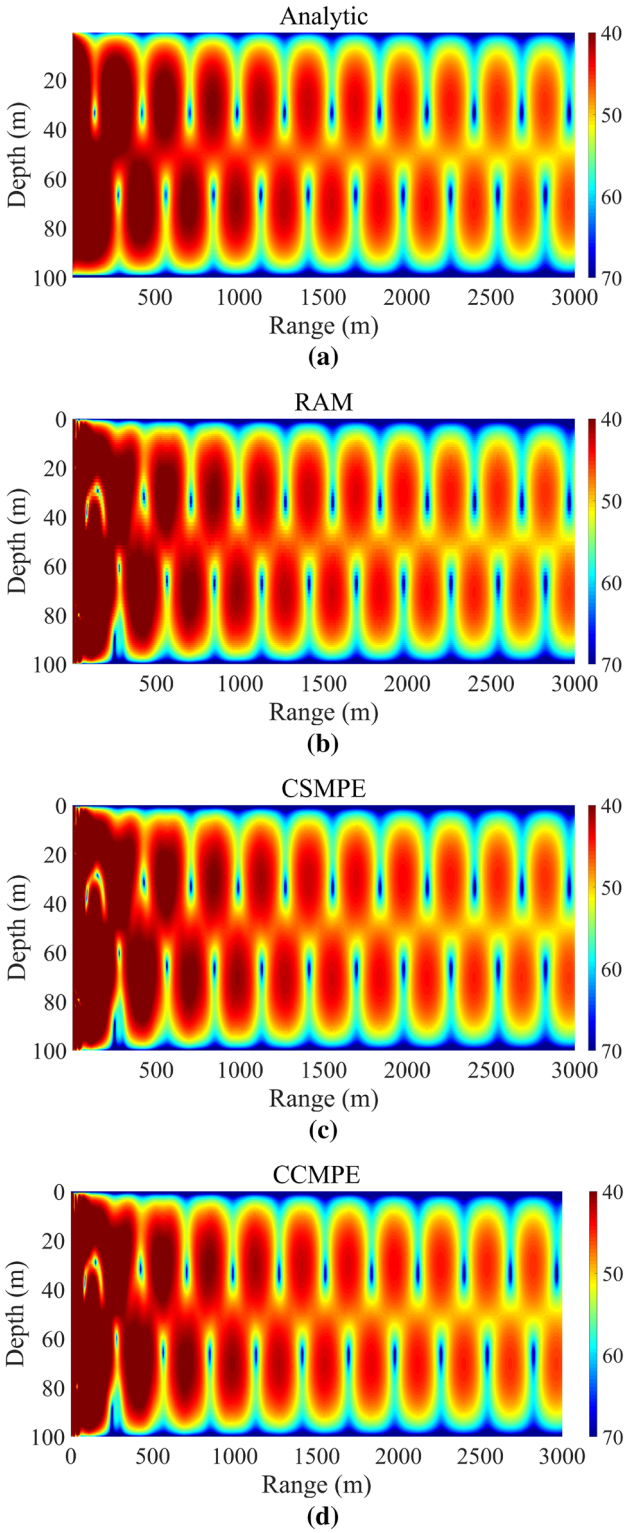

Fig. 2 TL fields of an ideal fluid waveguide in Experiment 1 calculated using analytical solution (**a**), the RAM (**b**), CSMPE (**c**) and CCMPE (**d**)

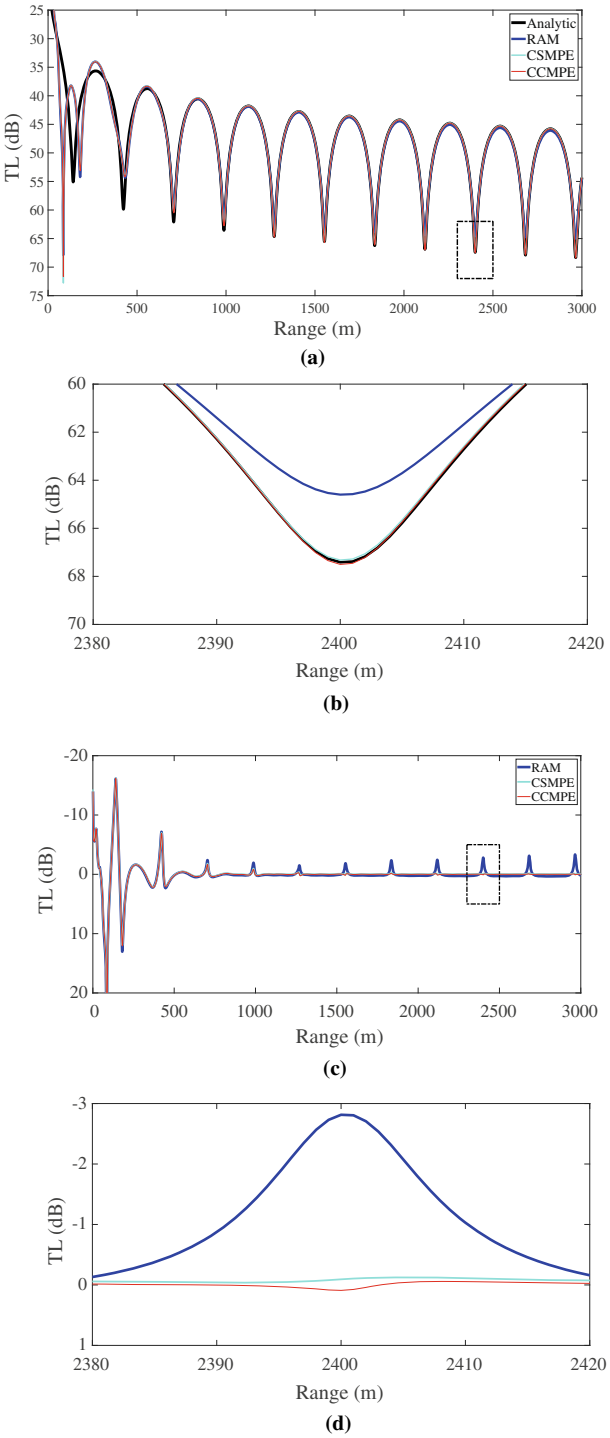

Fig. 3 The TL of Experiment 1 calculated by the four programs at a depth of 36 m (**a**) and the errors between the RAM, CSMPE and CCMPE programs and the analytical solution (**c**); (**b**) and (**d**) are the enlarged portions in the rectangles of (**a**) and (**c**), respectively

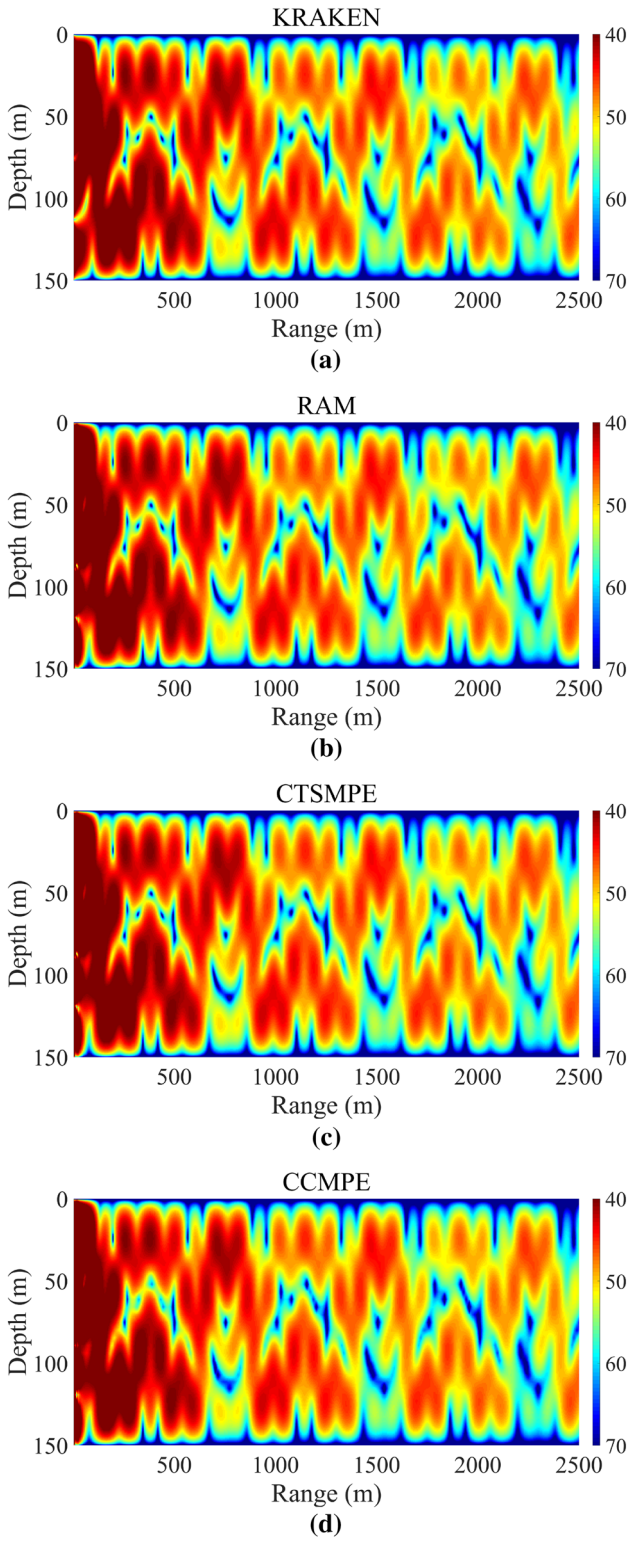

Fig. 4 TL field of Experiment 2 calculated using KRAKEN (**a**), the RAM (**b**), CSMPE (**c**) and CCMPE (**d**)

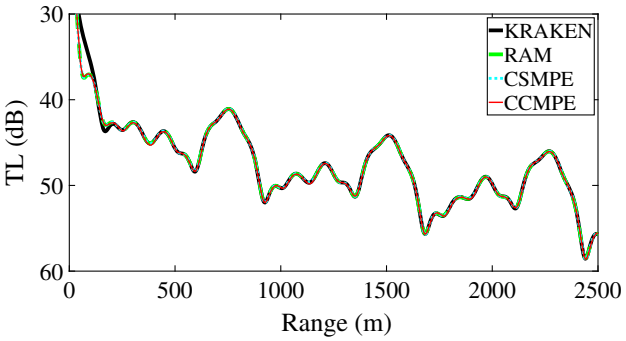

Fig. 5 The TL of Experiment 2 calculated by the four programs at a depth of 40 m

Hz are considered. Since this experiment does not have an analytical solution, we use the result of the FFP as a reference and compare only the relative differences among these three programs. A total of 5000 equally spaced discrete points are used in the vertical direction for FFP and the RAM, CSMPE uses $N = 600$, and CCMPE uses $N = 500$. Δr is taken as 20 m. It can be seen from Fig. 8 that the results of the four programs are very similar. The differences between the FFP and the other three programs appear in the near field, especially under the sound source. However, in other regions, the results of the four programs are in better agreement.

5 Discussion

In many cases, numerical acoustic fields have no exact analytical solutions, and the PE model still has errors in the near field due to omitting the inwardly propagating waves. Experiment 1 has an analytical solution, and the accuracy of various methods can be accurately compared. Therefore, we take Experiment 1 as an example. To accurately compare the sound fields calculated by various methods, the definition of a quantitative accuracy index is necessary. Taking into account the need to eliminate the sound field distortion caused by the backward waves, for Experiment 1, we select the TL at each discrete point in the range of 1500 m $\leq r \leq$3000 m, find the absolute error between the results calculated by various methods and the analytical solution and then find the mean value of the absolute error. The mean absolute error (MAE) defined in this way is used to measure the accuracy of the sound field calculated by various methods. Table 2 lists the MAEs calculated by the three methods under different numbers of discrete points. It can be seen from the table that as N increases, the errors of CSMPE and CCMPE gradually decrease, and their errors are approximately the same level. The error of RAM is much larger than that of CCMPE. Particularly in the configuration of Experiment 1, CCMPE takes $N = 50$ and RAM takes $M = 200$, where M is the number

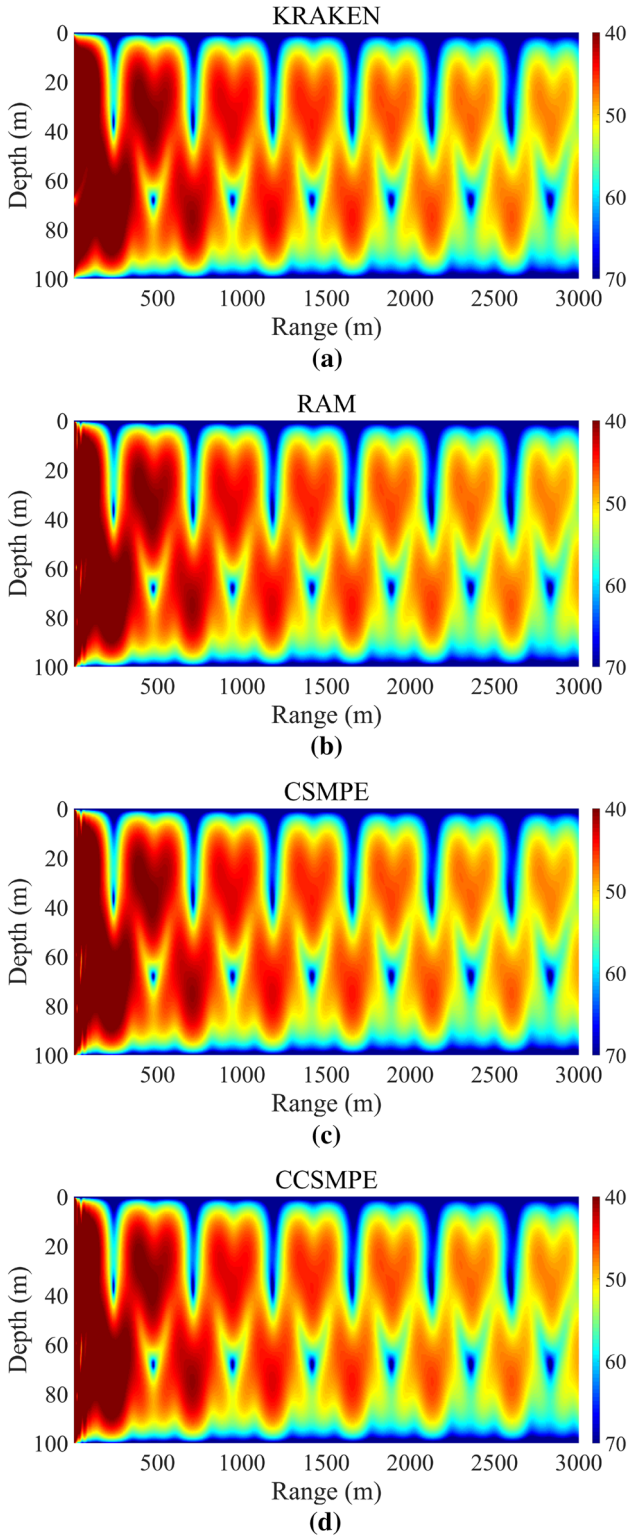

Fig. 6 TL field of Experiment 3 calculated using KRAKEN (**a**), the RAM (**b**), CSMPE (**c**) and CCMPE (**d**)

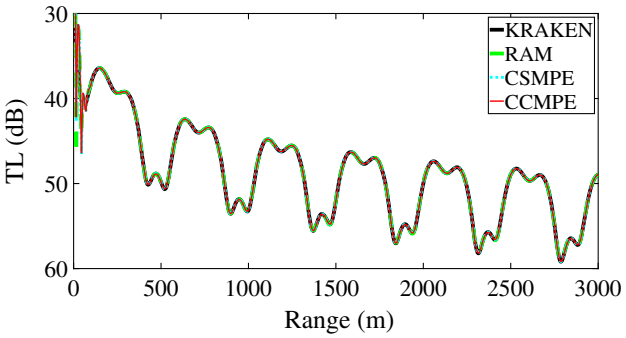

Fig. 7 The TL of Experiment 3 calculated by the four programs at a depth of 60 m

of discrete points of RAM. It can be seen that CCMPE uses fewer discrete points but obtains a more accurate solution than RAM.

It can also be seen from Table 2, for CCMPE and CSMPE, when N is set to 17, the accuracy of the calculation result is almost the same as when M in RAM is set to 400. Table 3 lists the running time of each program when the number of discrete points is different. CSMPE and CCMPE are both written in MATLAB, and the RAM has both a FORTRAN (ram1.5) version and a MATLAB version. The test platform is a Dell XPS 8930 desktop computer equipped with an Intel i7-8700K CPU and 16 GB memory. The FORTRAN compiler used in the test is gfortran 7.5.0, and the MATLAB version is 2019a. The results listed in the table are the average of ten runs. From the perspective of running time, when the same accuracy is reached, the running time of RAM is the shortest, followed by CCMPE, and the slowest is CSMPE.

From the analysis of the first experiment, we can see that in general, CCMPE uses fewer discrete points to match or exceed the RAM's accuracy, especially when the acoustical profiles are smooth. The smaller the number of discrete points in the vertical direction is, the shorter the running time. In the numerical experiments, the sound speed profiles of Experiments 1 and 4 are smooth, while those of Experiments 2 and 3 are rough. In actual calculations, for rough sound speed profiles, credible results can be obtained by increasing the number of collocation points N. In general, compared with the RAM, CCMPE has higher accuracy; the calculation speed of CCMPE is much faster than that of CSMPE when the accuracy is equivalent even though both of them are spectral methods.

It is worth noting that none of the four experiments above consider vertical changes in density or attenuation because the RAM program defaults to a water layer density of 1 g/cm^3 and an attenuation of 0 dB/λ. However, both CCMPE and CSMPE can address problems for which the density and attenuation change with depth. For the sound propagation under the long-range complex sound speed profile in the deep sea, the TL of the parabolic equation model has not

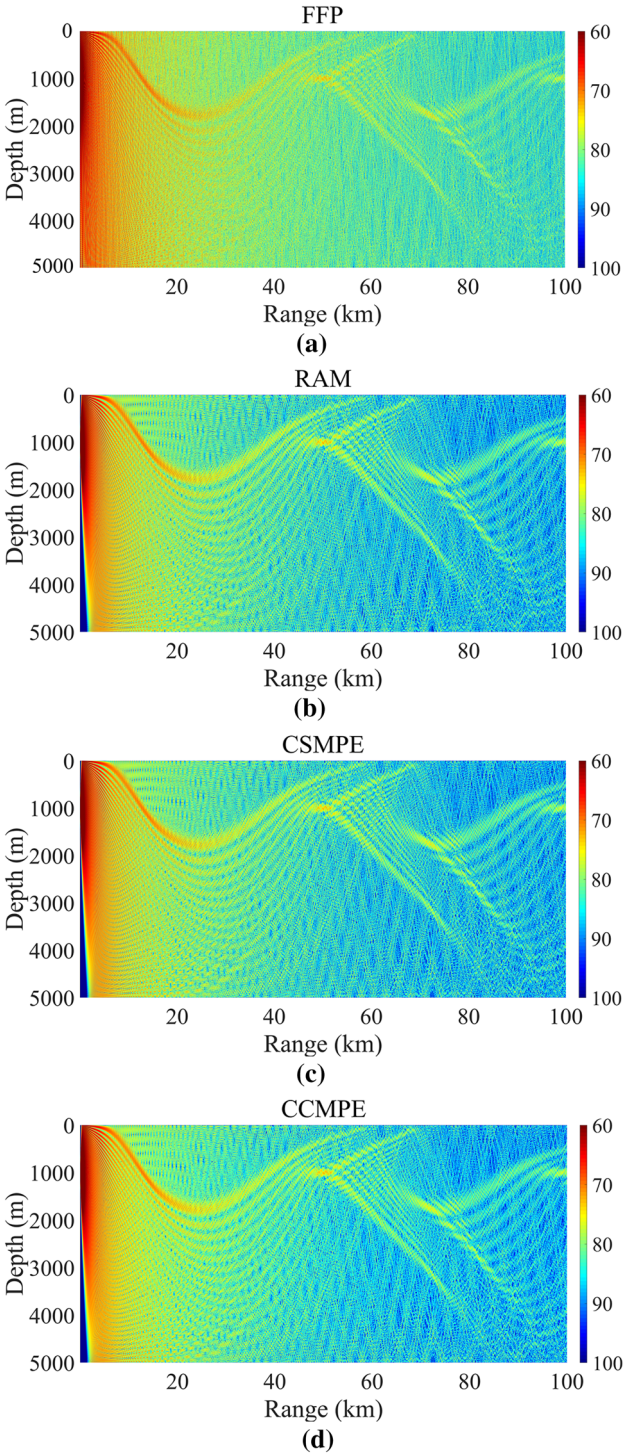

Fig. 8 TL field of Experiment 4 calculated using the FFP (**a**), the RAM (**b**), CSMPE (**c**) and CCMPE (**d**)

Table 2 The MAEs of the TL change with the numbers of discrete points in Experiment 1 (unit: dB)

FDM		Spectral Methods		
M	MAE	N	MAE	
	RAM		CSMPE	CCMPE
100	4.3022	17	1.8954	1.8122
200	2.4008	20	0.5223	0.5381
250	2.1672	50	0.0611	0.0641
400	1.8833	100	0.0407	0.0457

Table 3 The running times of the programs change with the number of discrete points in Experiment 1 (unit: sec)

FDM			Spectral Methods		
M	Time		N	Time	
	RAM	RAM (MATLAB)		CSMPE	CCMPE
100	0.1705	1.2293	17	0.5977	0.4852
200	0.2842	1.9136	20	0.6387	0.5271
250	0.3381	2.4045	50	1.6058	1.4510
400	0.5407	3.5442	100	4.6323	4.4502

only a magnitude error but also a phase error [1,36]. The MAE defined herein is only applicable to the simple case of Experiment 1 but not to the other experiments.

6 Conclusions

The CCM provides a program for computing the sound pressure field when the sea surface and bottom are range independent. This method first interpolates the acquired data of the sound speed, density and attenuation profiles to the CGL points. After modifying the depth operator matrix with the boundary conditions, complex matrix algebraic equations for solving the pressure field are formed that can be solved by applying numerical libraries and algorithms. The validity and reliability of the CCM are demonstrated in comparison with the FDM (RAM program) and Chebyshev–Tau spectral method (CSMPE program). From the perspective of computational speed, CCMPE is superior to CSMPE. From the perspective of computational accuracy, CCMPE is sufficiently high compared with the RAM and CSMPE. In cases where the sound speed, density and attenuation profiles are not sufficiently smooth, the CCM should use more CGL points to obtain convincing results. Furthermore, this article simply abstracts the ocean into a layer, but in the actual ocean, the sediment (which may be composed of silt or sand with completely different densities and attenuations) should be considered. Moreover, regarding the issue that the computational time is longer than that of the RAM, we aim to

decrease the running time through parallel computing technology in future work.

Acknowledgements This work was supported in part by the National Key Research and Development Program of China (2016YFC1401800), in part by the National Natural Science Foundation of China (61972406, 51709267) and in part by the Project of the National University of Defense Technology (4345161111L).

Compliance with ethical standards

Conflict of interest The authors declare that they have no conflict of interest.

References

1. Jensen, F.B., Kuperman, W.A., Porter, M.B., Schmidt, H.: Computational Ocean Acoustics. Springer, New York (2011)
2. Tappert, F.T.: The Parabolic Equation Approximation Method in Wave Propagation and Underwater Acoustics, vol. 70. Springer, New York (1977)
3. Desanto, J.A.: Relation between the solutions of the helmholtz and parabolic equations for sound propagation. J. Acoust. Soc. Am. **62**, 295–297 (1977)
4. Fain, G., Estes, L.E.: Numerical technique for computing the wide-angle acoustic field in an ocean with rang-dependent velocity profiles. J. Acoust. Soc. Am. **62**, 38–43 (1977)
5. Lee, D., Mcdaniel, S.T.: A finite-difference treatment of interface conditions for the parabolic wave equation: the horizontal interface. J. Acoust. Soc. Am. **71**, 855–858 (1982)
6. Jacobson, M.J., Robertson, J.S., Siegmann, W.L.: A treatment of three-dimensional underwater propagation through a steady shear flow. J. Acoust. Soc. Am. **86**, 1484–1489 (1989)
7. Wang, D.P., Wang, C.W.: Application of parabolic equation model to shallow water acoustic propagation,in environmental acoustics. World Sci. pp 755–792 (1994)
8. Collins, M.D.: Higher-order pade approximations for accurate and stable elastic parabolic equations with applications to interface wave propagation. J. Acoust. Soc. Am. **89**, 1050–1057 (1991)
9. Thomson, D.J.: Wide-angle parabolic equation solutions to range-dependent benchmark problems. J. Acoust. Soc. Am. **87**, 1514–1520 (1990)
10. Collins, M.D.: A self-starter for the parabolic equation method. J. Acoust. Soc. Am. **92**, 2069–2074 (1992)
11. Spiesberger, J.L., Boden, L., Bowlin, J.B.: Time domain analysis of normal mode, parabolic, and ray solutions of the wave equation. J. Acoust. Soc. Am. **90**, 954–958 (1991)
12. Salomons, E.M.: Improved green's function parabolic equation method for atmospheric sound propagation. J. Acoust. Soc. Am. **104**, 100–111 (1998)
13. Collins, M.D., Siegmann, W.L.: A complete energy conserving correction for the elastic parabolic equation. J. Acoust. Soc. Am. **105**, 687–692 (1999)
14. Collins, M.D.: User's guide for RAM versions 1.0 and 1.0p (1999). https://oalib-acoustics.org/PE/index.html
15. Henderson, L.: FOR3D (2015). https://oalib-acoustics.org/PE/index.html
16. Shang, E.C., Lee, D., Pierce, A.D.: Parabolic equation development in the twentieth century. J. Comput. Acoust. **8**, 4 (2000)
17. Zheng, Q.L.: Experiments on the 30-day long-range numerical weather prediction in a seven-level spectral model. J. Acad. Meteorol. Sci. **10**, 234–246 (1989)
18. Hu, Z.D., Ding, H.B., Cao, Y.: Application of pseudo-spectral method in rapid orbit optimization for SGKW. Aerospace Control (2009)
19. Boyd, J.P.: Chebyshev and Fourier Spectral Methods, 2nd edn. Dover, New York (2001)
20. Nuttawit, W., Arisara, C., Sacharuck, P.: Chebyshev collocation approach for vibration analysis of functionally graded porous beams based on third-order shear deformation theory. Acta Mech. Sin. **34**(6), 1124–1135 (2018)
21. Sinan, D., Mehmet, S.: Rational chebyshev collocation method for solving nonlinear heat transfer equations. Int. Commun. Heat Mass Transf. **114**, 104595 (2020)
22. Wang, Y.Q., Zhao, H.L.: Free vibration analysis of metal foam core sandwich beams on elastic foundation using chebyshev collocation method. Arch. Appl. Mech. (2019)
23. Khaneh, M.P., Ovesy, H.R.: Chebyshev collocation method for static intrinsic equations of geometrically exact beams. Int. J. Solids Struct. (2014)
24. Evans, R.B., Di X., Kenneth, E.G.: A Legendre–Galerkin technique for differential eigenvalue problems with complex and discontinuous coefficients, arising in underwater acoustics (2020)
25. Tu, H., Wang, Y., Liu, W., Ma, X., Xiao, W., Lan, Q.: A chebyshev spectral method for normal mode and parabolic equation models in underwater acoustics. Math. Prob. Eng. **2020**, 1–12 (2020)
26. Tu, H., Wang, Y., Lan, Q., Liu, W., Xiao, W., Ma, S.: A chebyshev-tau spectral method for normal modes of underwater sound propagation with a layered marine environment. J. Sound Vib. **492**, 1–16 (2021)
27. Tu, H.: A Chebyshev-Tau spectral method for normal modes of underwater sound propagation with a layered marine environment in matlab and fortran (2021). https://oalib-acoustics.org/Modes/NM-CT/
28. Tu, H., Wang, Y., Ma, X., Zhu, X.: Applying chebyshev-tau spectral method to solve the parabolic equation model of wide-angle rational approximation in ocean acoustics. arXiv:2012.02405 (2020)
29. Colbrook, M.J., Ayton, L.J.: A spectral collocation method for acoustic scattering by multiple elastic plates. J. Sound Vib. **461**, 114904 (2019)
30. Jie, S., Tao, T., Lilian, W.: Spectral Methods Algorithms, Analysis and Applications. Springer, Berlin (2011)
31. Gottlieb, David, Orszag, Steven A.: Numerical analysis of spectral methods, theory and applications. Society for Industrial and Applied Mathematics, Philadelphia (1977)
32. Canuto, C., Hussaini, M.Y., Quarteroni, A., Zang, T.A.: Spectral Methods Fundamentals in Single Domains. Spring, Berlin (2006)
33. Zhang, Z.: Super convergence of a chebyshev spectral collocation method. J. Sci. Comput. **34**, 237–246 (2008)
34. Porter, M.B.: The Kraken Normal Mode Program. SACLANT Undersea Research Centre (2001). https://oalib-acoustics.org/Modes/Kraken/
35. Chowdhury, A.D., Vendhan, C.P., Bhattacharyya, S.K., Mudaliar, S.: A Rayleigh-Ritz model for the depth eigenproblem of heterogeneous pekeris waveguides. Acta Acust. United Acust. **104**, 597–610 (2018)
36. Yang, K., Lei, B., Lu, Y.: Principle and Application of Typical Sound Field Model of Ocean Acoustics (in Chinese). Northwestern Polytechnical University Press, Xi'an (2018)